Simulation Study of Sulfonate Cluster Swelling in Ionomers.

Elshad Allahyarov

Department of Physics, Case Western Reserve University, Cleveland, 44106 Ohio, USA

OIVTRAN, Joint Laboratory of Soft Matter, Moscow, 127412 Russia,

HHU Düsseldorf, Institut für Theoretische Physik II,

Universitätstrasse 1, 40225 Düsseldorf, Germany

Philip L. Taylor

Department of Physics, Case Western Reserve University, Cleveland, Ohio 44106, USA

Hartmut Löwen

HHU Düsseldorf, Institut für Theoretische Physik II,

Universitätstrasse 1, 40225 Düsseldorf, Germany

Abstract

We have performed simulations to study how increasing humidity affects the structure of Nafion-like ionomers under conditions of low sulfonate concentration and low humidity. At the onset of membrane hydration, the clusters split into smaller parts. These subsequently swell, but then maintain constant the number of sulfonates per cluster. We find that the distribution of water in low-sulfonate membranes depends strongly on the sulfonate concentration. For a relatively low sulfonate concentration, nearly all the side-chain terminal groups are within cluster formations, and the average water loading per cluster matches the water content of membrane. However, for a relatively higher sulfonate concentration the water-to-sulfonate ratio becomes non-uniform. The clusters become wetter, while the inter-cluster bridges become drier. We note the formation of unusual shells of water-rich material that surround the sulfonate clusters.

I. INTRODUCTION

An interest in ionomers, i.e. ion-containing polymers, began fifty years ago with the development of organic ion-exchange resins [1]. The properties of these materials are completely different from those of other polymers as a consequence of the ionization of the ionic groups in polar solvents. The specificity of the interaction between the ion, the solvent, and the polymer makes it possible for these materials to be used as perm-selective membranes, thermoplastics or films for micro-encapsulation and coating [2]. A significant interest in ionomer materials also stems from their growing application as a polymer electrolyte membrane (PEM) or a proton exchange membrane in fuel cell technology [3, 4, 5, 6].

DuPont de Nemours was the first manufacturer in the early 1960s to develop a perfluorosulfonic membrane commercially [7, 8]. This membrane, which was named Nafion®, consists of a polytetrafluoroethylene hydrophobic backbone to which perfluorovinyl ether pendant side chains are attached at more or less equally spaced intervals. The pendant chains are terminated by sulfonic head groups SO_3H, and these are responsible for the large variety of microstructures in which the ionomer can be assembled. When exposed to humidity, the membrane takes up large amounts of water, leading to the dissociation of the acid groups $SO_3H \rightarrow SO_3^- + H^+$ and to the formation of a nanophase-separated network of aqueous (hydrophilic) clusters and hydrophobic polymer. According to the cluster morphology model of Hsu and Gierke [9], spherical clusters are uniformly distributed throughout the material and are interconnected by channels [10, 11]. Subsequent cluster-based models, such as the Mauritz-Hopfinger model [12, 13], the Yeager three-phase model [14], the Eisenberg model of clusters of hydrocarbon ionomers [15], and the Litt model of a lamellar morphology for sulfonate domains [16], have tried to quantify the cluster radius and spacing as a function of the polymer equivalent weight and the hydration level. Other structural models were proposed to describe the membrane swelling process from a dry state to a colloidal suspension as a continuous process [17, 18].

There is still ongoing debate about which one of the proposed models is more suitable and effective in representing the ionomer's conductivity through its nanophase separated network of hydrophilic regions. The issue is complicated by the fact that experimental

studies show the ionomer structure to depend on the pretreatment methods used in its preparation [8, 19, 20, 21, 22, 23]. The membrane pretreatment serves to reduce the remnant anisotropy in the morphology of extruded membranes, and to clean a solvent-cast membrane from impurities [13, 24]. Rigorously speaking, the question of how the pretreatment steps, such as swelling and/or boiling in solvents, annealing, rinsing in water, drying in vacuum/air, and the order of these steps, affect the membrane morphology, is not yet answered. Most of the pretreatment protocols have the ultimate goal of improving the water uptake of the membrane [20, 25]. For example, in Ref. [20] it has been shown that the water uptake of a dry membrane depends on how it was dried from its swollen state at elevated temperatures. If it was first cooled and then dried, then the membrane keeps its swollen volume. But if it was first dried and then cooled, the membrane shrinks in volume during the drying process. As a result, the outcome of the first protocol is a membrane that takes up a desirably large amount of water, and thus has a better proton conductivity.

The water solvation of a PEM, which is necessary for its efficient operation, reduces its working temperature range: the membrane will not be exploitable at freezing and boiling water temperatures. A possible way to overcome this limitation is the development of new membranes that can operate at the low wetting conditions where λ, which is the number of water molecules per sulfonate group, is less than five. In the case of full hydration there are 5 water molecules in the primary hydration shell of a sulfonate [26, 27, 28]. In low-humidity membranes, the protons diffuse along narrow pathways near the SO_3^- terminals of side chains, and two conflicting effects come into play. On the one hand, the proximity of negatively charged sulfonates considerably suppresses the mobility of the protons. On the other hand, when the separation distance between sulfonates is small, the activation energy for proton hopping between adjacent end-groups becomes comparable with the activation energy in the bulk water [29], making the net result unclear. The proton mobility in low-humidity membranes can be also elevated by adding flexibility to the sidechains, and by modifying the network structure of sidechain clusters.

Despite the fact that various models have emerged to explain the properties of hydrated Nafion membranes, a systematic study of how the molar concentration η of sulfonate head groups and the solvent content parameter λ affect the network structure of sulfonates, and particularly the swelling of single clusters has not yet appeared. This absence is important for understanding proton transport and the onset of percolation in low-humidity membranes,

and forms the motivation for this study.

Here we perform simulations to investigate the dependence of the cluster swelling on the hydration level λ and the sulfonate molar concentration η of the membrane by employing different sidechain architecture models. We restrict ourselves to the case of ionomers for which there is no bulk water inside the sulfonate clusters, and in which the sulfonate concentration is considerably below the percolation limit for the head groups. It is expected that in these *low-humidity* and *low-sulfonate* membranes no overlapping between sulfonate clusters takes place. In order to distinguish a sulfonate cluster from a water cluster, which is necessary in the interpretation of our simulation results, for the former we adopt the term "sulfonate multiplet", first introduced by Eisenberg in Ref. [15] to describe the primary aggregates of sulfonates. We show that at the onset of swelling, which is defined as the transition from a dry multiplet into a wet multiplet with dissociated protons, the multiplets split into smaller parts. The solvation of these resultant multiplets is analyzed for different hydration levels and sulfonate concentrations. In particular, we will demonstrate the formation of water shells around the sulfonate multiplets.

The paper is organized as follows. In Section II we briefly discuss the benefits of using coarse-grained models (as opposed to all-atomistic approaches), and describe the coarse-grained model and system parameters employed here. The simulation details are outlined in Section III. Results on multiplet formation in dry and solvated membranes, water shells around multiplets, ionomer deformation, and proton diffusion are discussed in Section IV. We conclude in Section V.

II.   COARSE-GRAINED SYSTEM PARAMETERS

Despite the rich variety of experimental findings and theoretical predictions for the ordered morphology in PEM materials, numerical experiments have so far had little success in finding any clear picture of cluster formation in hydrated membranes. The main reason for this is the fact that individual ionic clusters are about 2–5 nm in size, and this is usually comparable to, or even larger than, the system sizes affordable in all-atomistic modeling. As a result, atomistic simulations, which are quite helpful for understanding the simple pore physics and small ionomer molecular conformations, are not able to capture the distribution of sulfonate clusters in the hydrophobic matrix. However, as already outlined in the

introduction, a knowledge of this distribution is crucial for the determination of the ionomer connectivity and the proton conductivity of the PEM material.

Fortunately polymers show a large degree of universality in their static and dynamic behavior. The universal scaling properties of the ionomer as a function of chain length, sulfonate density, and membrane composition can be most efficiently studied via coarse-grained molecular models. One of the most commonly employed systems is a bead-spring model, where each bead represents a segment of a realistic chain. Wescott et al [30] and Vishnyakov et al [31] have simulated large ionomer systems using coarse-grained approaches in which an entire sidechain was represented by a nanometer-size hydrophilic blob. Their simulations report irregularly shaped hydrophilic clusters embedded into the polymeric matrix of backbone chains. While such gross coarse-graining is computationally convenient, it is not possible to draw firm conclusions regarding proton diffusion from the conformational results obtained for the polymer. It is therefore necessary to limit the coarse-graining approach to the level at which the sulfonic acid groups of the polymer can be explicitly treated, as these groups contain the essential membrane-specific interaction sites relevant to absorbed water and conducting protons.

In our 'united atom' approximation for Nafion, the ether oxygens and sulfur atoms are treated individually, while the fluorocarbon groups are consolidated as a single particle, as are the three oxygens of the sulfonate [32, 33, 34]. The fluorocarbon groups, the sulfonate oxygens, and the sulfur atoms are modeled as single Lennard-Jones (LJ) particles with a diameter σ= 0.35 nm. The protons carry the full formal charge of $Q_p = +e$, the sulfur atoms have $Q_S = +1.1e$, and the combined triplet of oxygen atoms carries $Q_{O_3} = -2.1e$. The partial charges of the ether oxygens and the fluorocarbon LJ particles are set to zero. Depending on whether the membrane is dry or hydrated, two different representations have been used for the sulfonate head groups. For dry membranes, we implement an attached-proton model, also called a dipole model for head groups, which was extensively analyzed in our previous paper [32]. Though the attached-proton model does not allow for proton diffusion, it is considered as a good starting point for a step-by-step exploration of nanophase morphology in PEM materials. For the hydrated ionomer we assume a detached-proton model [33, 35], where the protons diffuse freely in the system, where they interact with ionized head groups and water molecules.

The configurational part of the coarse-grained Hamiltonian for the attached and detached

proton models is a combination of Coulomb interactions, non-bonded, and bonded interactions between all the ionomer components:

$$U_{\text{total}} = U_{LJ} + U_Q + U_{\text{bond}} + U_{\text{angle}} + U_{\text{dihedral}} \ . \tag{1}$$

Here $U_{\text{total}}, U_{LJ}, U_Q, U_{\text{bond}}, U_{\text{angle}}$ and U_{dihedral} are the total potential energy and its Lennard-Jones, electrostatic, bond-stretching (bond-length term), angle bending (bond-angle term) and dihedral angle components, respectively:

$$U_{LJ}(r) = 4\varepsilon_{LJ} \sum_{i>j} \left((\sigma/r_{ij})^{12} - a(\sigma/r_{ij})^6 \right), \tag{2}$$

$$U_Q = \sum_{i>j} \frac{Q_i Q_j}{\epsilon r i j}, \tag{3}$$

$$U_{\text{bond}}(r) = \frac{1}{2} \sum_{\text{all bonds}} k_b (r - r_0)^2, \tag{4}$$

$$U_{\text{angle}}(\theta) = \frac{1}{2} \sum_{\text{all angles}} k_\theta (\theta - \theta_0)^2, \tag{5}$$

$$U_{\text{dihedral}}(\alpha) = \frac{1}{2} \sum_{\text{all dihedrals}} k_\alpha \left(1 - d\cos(3\alpha)\right). \tag{6}$$

In Eq.(2) the LJ interaction coefficient ε_{LJ} in units of $k_B T$ was chosen to be 0.33. The parameter a in the LJ term is 1 for hydrophobic-hydrophobic (HH) interactions, and 0.5 for hydrophobic-hydrophilic (HP) interactions and hydrophilic-hydrophilic (PP) interactions. In the latter case only the repulsive part of the LJ potential (a shifted LJ potential for $r < 1.1224\sigma$) has been considered. In Eq.(3), Q_i and Q_j are the electrostatic charges of the two interacting elements, which can be sulfur atoms, oxygen triplets, protons, or the hydrogens or oxygen of the water molecules, and ϵ is the dielectric constant of the ionomer. In Eqs.(4)–(6) the following force-field parameters have been used: the equilibrium bending angle $\theta_0 = 110^0$, the equilibrium bond length $r_0 = 0.44\sigma$, the bending force constant $k_\theta = 120\frac{\text{kcal}}{\text{mol deg}^2}$ and the stretching force constant $k_b = 7 \times 10^4 \frac{\text{kcal}}{\text{mol(nm)}^2}$. The dihedral angle parameters were $d = -1$ (+1) and $k_\alpha = 10.8 k_B T$ ($k_\alpha = 3.7 k_B T$) for the backbone (sidechain) segments.

The dielectric properties of the coarse-grained material are represented by a distance-dependent dielectric function,

$$\epsilon(r) = 1 + \epsilon_B (1 - r/\sigma))^{10}/(1 + (r/\sigma)^{10}), \tag{7}$$

6

where ϵ_B is the bulk dielectric constants of the ionomer. Usually a uniform permittivity $\epsilon = 1$, or equivalently $\epsilon_B = 0$ in Eq.(7), is accepted in *ab initio* quantum-mechanical simulations, where all the ionomer atoms are explicitly taken into account. Since the coarse-grained approach neglects the atomistic structure of the ionomer monomers, additional approximations for the dielectric permittivity have to be made to account for the polarization effects of the ionomer monomers as a response to the strong electrostatic fields of the sulfonate groups and protons. To be accurate, $\epsilon(r)$ should depend upon the atom types and the absolute values of all the explicit coordinates. The problem, of course, is that the specific form of $\epsilon(r)$ is not known. For the bulk dielectric constant ϵ_B we use $\epsilon_B=8$, which is appropriate to the dielectric permittivity of Nafion as measured in high-frequency studies [19] and differential scanning calorimetry [36], and from first-principle calculations [37].

Taking into account the fact that the sulfonic acid tips of sidechains are hydrophilic, and the remaining part of sidechains, as well as the backbone polymer, are hydrophobic [38, 39], we use the following notation to describe the polymer architecture: $n_1 H + n_2 P$ for sidechains and $n_3 H$ for the backbone segments. Here n_1 is the number of hydrophobic monomers per sidechain, n_2 is the number of hydrophilic monomers per sidechain, and n_3 is the number of backbone monomers between two adjacent sidechains. The total number of sidechain monomers per pendant chain is $n_1 + n_2$ in the detached proton model, and $n_1 + n_2 + 1$ in the attached-proton model. The key variables that describe our model ionomer system are listed in Table I.

III. SIMULATION DETAILS

Extensive coarse-grained molecular dynamics simulations were performed to investigate the swelling properties of sulfonate multiplets at four different solvation parameters λ and two distinct sulfonate molar concentrations η. The parameter η is defined as $\eta \equiv (N_S/N_0) V$, where N_S is the number of sidechains in the volume $V = L^3$ of the simulation cell, and N_0 is Avogadro's number. Whereas in experimental studies the parameters η and λ are coupled to each other [40], in numerical simulations both quantities can be changed independently. A series of simulation runs are summarized in Table II. The molar concentrations $\eta_1=0.8$ mol/l and $\eta_2=1.5$ mol/l correspond to the backbone segment lengths $n_3=50$ and $n_3=20$ respectively. Varying the parameter η, i.e. varying the chain volume per SO_3^- group, is

in some ways equivalent to simulating materials with different equivalent weights [40]. For convenience, we will refer to the membrane with sulfonic molar concentration η as 'membrane η'. In most simulations of Nafion-like ionomers the parameter n_3 is usually varied between 14 and 18. Shorter segments with n_3=10 have been considered in the atomistic simulations of Ref. [41], and longer segments n_3=30 in the coarse-grained approaches of Ref. [31]. In the latter case the nearest-neighbor distance between the sulfonate multiplets is large. Thus our choice of a larger n_3 makes possible the investigation of the solvation properties of single multiplets in slightly hydrated membranes.

There were $N = (n_1 + n_2 + n_3) \times N_S$ polymer monomers in the simulation box of length L. All simulations were carried out for both the $n_1 = 7$ and $n_2 = 2$ sidechain architectures. The number of sidechains N_S was 500 for membrane η_1 and 1000 for membrane η_2. The negative charges of N_S sulfonate groups were compensated by N_S positive protons to guarantee an overall charge neutrality in the system. Simulations with explicit water include an additional $3 \times \lambda \times N_S$ water charges, as we are using the SPC solvent model [42, 43]. The box size L was systematically increased from $L = 30\sigma$ to $L = 32.5\sigma$ when the water content λ was increased from λ=0 to λ=5 in order to keep the density of the hydrated membrane constant.

One of the main challenges in generic ionomer simulations is the fact that the ionomer molecule is quite stiff at ambient temperatures and low humidity conditions. In experimental studies a fast ionomer equilibration is usually achieved through different pretreatments protocols, such as a soaking in a solvent or high-temperature annealing. These steps improve the sidechain kinetics and decrease the barrier between the trapped metastable states and the low-lying states at the global minimum in free energy. Overall, a full equilibration, even after these pretreatment steps, takes hours or days, a time span that is far beyond the feasible simulation times of several nanoseconds in typical molecular dynamics runs. To overcome this obstacle we implemented the following artificial steps [44]:

a) the sidechains were temporarily detached from the backbone skeleton, a technique that has been successfully applied in Refs. [33, 35, 45, 46, 47],

b) the skeleton was cut into smaller segments of length n_3.

The resulting 'fragmented' ionomer reaches the equilibrium state very fast because of the increased diffusive movement of its segments. Typical MD runs of 500 ps duration in the NVT ensemble were enough to fully equilibrate the simulated system. The system temperature T was controlled by coupling the ionomer to a Langevin thermostat with a friction

coefficient $\gamma = 10\text{ps}^{-1}$ and a Gaussian white-noise force of strength $6k_BT\gamma$. The equations of motion were integrated using the velocity Verlet algorithm with a time step of 0.25 fs. We also imposed standard periodic boundary conditions to our system, thus filling space with translational replications of a fundamental cell. Long-range electrostatic interactions were treated using the Lekner summation algorithm [48].

In the next stage of the simulations, the ionomer segments were reassembled back into a branched chain characterizing the original Nafion-like ionomer. This was achieved by a simultaneous introduction of bonds and angular constraints between the ends of backbone segments unifying them into a single and long backbone chain. Similar bond and angular constraints were introduced between the fluorocarbon tail monomers of detached sidechains and the median section monomers of backbone segments. To avoid the formation of unphysical star-like branches only a single occupancy of backbone attachment sites was permitted. The simulations were then resumed for another few hundred picoseconds until a new equilibrium state was reached. Then the statistically averaged quantities of interest were gathered during the next 3ns–5ns of the long production runs.

IV. SIMULATION RESULTS

A. Multiplet formations in dry and solvated membranes

A typical snapshot of a hydrated membrane from Run 3 is shown in Figure 1. The backbone skeleton, plotted as lines, creates a hydrophobic network with chaotically scattered pores. These pores incorporate micelle-like clusters of sidechain sulfonates (shown as spheres), which are filled with water molecules and protons. The number densities $\rho(\vec{r})$ of the hydrophobic part of the ionomer and of the absorbed water, averaged over a 100 fs run, are shown in Figure 2 and Figure 3, respectively. The density $\rho(\vec{r})$ corresponds to the probability of finding a particular membrane component, hydrophobic monomer or hydrophilic water, at the point $\vec{r}$ during a short simulation run. The quasi-regular network of polymer skeleton with interconnected hydrophilic pores changes its form slowly with time.

The structure of the sulfonate multiplets was probed through the calculation of the sulfonate-sulfonate pair correlation function,

$$g_{SS}(r) = \frac{V}{N_S}\frac{dn_S(r)}{4\pi r^2 dr} \quad . \tag{8}$$

Here $dn_S(r)$ is the number of sulfurs located at the distance r in a shell of a thickness dr from a fixed sulfur atom. The function $g_{SS}(r)$ indicates the probability of finding two sulfonate monomers at a separation distance r averaged over the equilibrium trajectory of the simulated system. Simulation results for $g_{SS}(r)$ for Runs 1–4 from Table II are shown in Figure 4. The dry multiplets have no detectable internal structure except the strong maximum at $r \approx 1.4\sigma$. In hydrated membranes the correlation function g_{SS} shows shell-like oscillations, a recognizable fingerprint of solvation shells. The first maximum of $g_{SS}(r)$ corresponds to the closest-approach configuration between neighboring sulfonates. The second peak of $g_{SS}(r)$ stems from a configuration where two neighboring sulfonates are separated by single proton or water molecule. Finally, the third peak of $g_{SS}(r)$ is related to configurations with more than one proton or water molecule between sulfonates. The dependence of the intensity of the correlations between the head groups on water content λ is due to the dielectric screening properties of water: the more the water content in the membrane, the weaker the sulfonate-sulfonate interactions. Similar results have been reported in the simulation results of Refs. [49, 50, 51, 52]. The greatly reduced intensity of the first peak of $g_{SS}(r)$ at $\lambda = 5$ can be understood as the onset of the improbability of the closest-approach sulfonate-sulfonate configurations in hydrated multiplets.

We determine the size of a multiplet as the position of the global minimum R_A^S (also known as the radius of the first coordination sphere) of the pair correlation functions g_{SS} in Figure 4. This position depends on the membrane hydration level λ, and can be used to calculate the number of head groups χ_S inside the multiplet according to the following relation

$$\chi_S = \frac{N_S}{V} \int_0^{R_A^S} g_{SS}(r) 4\pi r^2 dr. \tag{9}$$

The calculated values for the parameters R_A^S and χ_S are given in Table III for the membranes η_1 and η_2. There is a clear indication of the fact that the multiplets shrink in size at the onset of membrane solvation, which corresponds to the transition from Run 1 to Run 2. This shrinking, which is not in accord with the classical theories of cluster swelling in ionomers, is accompanied by a multiplet splitting into smaller parts. For instance, the dry multiplet in the membrane η_2 has a size $R_A^S = 5\sigma$ and consists of $\chi_S = 22$ head groups. Following hydration by a water content as low as $\lambda = 1$, this multiplet effectively splits into two smaller parts of size $R_A^S = 4.2\sigma$, each of them consisting of only 13 head groups. These small multiplets will consequently swell, keeping the number of their sulfonate population

constant, when additional water is absorbed into the membrane. The swelling radius is largely determined by the competition between two different internal energies, the elastic energy of the backbone material and the electrostatic energy of the pendant groups.

The pair correlation functions $g_{SS}(r)$ for two different sulfonate concentrations η_1 and η_2 are plotted in Figure 5. When the parameter η decreases, (as seen by a comparison of the thin and thick lines in Figure 5), the intensity of sulfur-sulfur correlations increases. This effect stems from the interplay between the electrostatic screening length l_D and the average separation distance $\bar{l}$ between the sulfonates. For an ionomer with a high sulfonate concentration η, one generally has $l_D < \bar{l}$, and thus the electrostatic correlations between the sulfonates are negligible. In this case a nanophase separation in the membrane is possible only due to the hydrophobic/hydrophilic immiscibility between the backbone and sidechain segments of the membrane. In the opposite case, when η is small and $l_D > \bar{l}$, the Coulomb correlations become sufficiently strong to force the sulfonates to form compact multiplets.

B. Separation distance between multiplets

It is a well established fact that the nearest-neighbor separation distance between the multiplets and the connectivity of multiplets into a network of hydrophilic pathways are the main contributing factors to the transport properties of ionomers. The typical multiplet-multiplet nearest-neighbor distances can be directly deduced from the density-density correlations in the network of head groups by consideration of the structure factor,

$$S(\vec{q}) = N_S^{-1} \left\langle \left[\sum_{i=1}^{N_S} \cos(\vec{q}\vec{r_i}) \right]^2 + \left[\sum_{i=1}^{N_S} \sin(\vec{q}\vec{r_i}) \right]^2 \right\rangle. \tag{10}$$

When there is no preferential ordering of the hydrophilic domains in the membrane, the structure factor of the sulfonates is isotropic, and hence depends only on the modulus $q = |\vec{q}|$ of the wave-vector. The calculated structure factors $S(q)$ for the dry and hydrated membranes are presented in Figure 6. The ionomer-peak position in the low q-region corresponds to the length of the density-density correlations $\overline{R} = 2\pi/q$ of sulfonates [17, 40, 53, 54].

The nearest-neighbor distance between the multiplets can also be deduced, though less precisely, from the position of the long-range maximum R_B^S of the pair correlation functions $g_{SS}(r)$ in Figure 4. As in the multiplet splitting effect, corresponding to the reduction in the multiplet size R_A^S at the onset of membrane solvation, the nearest-neighbor distance

11

R_B^S also decreases to smaller values according to the results of Run 1 and Run 2. This is a consequence of the increase in the multiplet population $\xi = N_S/\chi_S$. For example, the number of multiplets in the membrane η_1 increases from $\xi=30$ in the dry membrane to $\xi=50$ in the hydrated membrane. The calculated values for $\overline{R}$ and R_B^S, seen in Table III, match each other perfectly. We note that the increase of the average multiplet separation distance $\overline{R}$ for Runs 2–4 is a clear sign of membrane swelling, which is in accord with the results of Refs. [3, 40, 49].

C. Swollen multiplets inside a water shell

The pair correlation and the structure factor analysis, implemented in the previous subsection, can be also exploited to examine the water clustering features in hydrated membranes for Runs 2–4. We calculate the size of the water cluster R_A^W from the water-water correlation $g_{WW}(r)$ shown in Figure 7. The nearest-neighbor cluster separation distances R_B^W were evaluated from the water-water structure factors. The calculated values for both parameters are given in Table III. There is good agreement between the water-water and the sulfonate-sulfonate multiplet nearest-neighbor distances R_B^W and R_B^S. This is an indirect verification of the fact that the ionomer cluster is a mixture of sulfonates and absorbed water molecules. The distribution of water molecules inside the ionomer cluster can be analyzed by comparing the water cluster size R_A^W with the sulfonate multiplet size R_A^S. Whereas for the membrane η_1 there is an excellent match between these two parameters, for the membrane η_2 the water clusters are consistently bigger than the sulfonate multiplets. Based on this result we conclude that a part of the total water loading per multiplet in fact exists outside the multiplet boundaries. This 'outer' water shell encapsulates the multiplet and facilitates the formation of narrow water channels between the swollen multiplets. These channels, clearly seen in Figure 3, are the pathways through which the ionomer absorbs more solvent upon its hydration. The water channels are also an attractive place for the unclustered head groups, and assist the proton diffusion between neighboring multiplets. We remark that free bulk-like water would form in the interior of the multiplet only at sufficiently high solvation levels λ [55], a case not considered in this work.

The average number of water molecules χ_W per water cluster was calculated by using Eq.(9) for $g_{WW}(r)$. This parameter, together with the parameter describing the water-per-

sulfonate ratio χ_W/χ_S are given in Table III. For the membrane η_1 we obtain $\chi_W/\chi_S = \lambda$, a predicted result for the ionomer cluster with $R_A^W = R_A^S$. However for the membrane η_2 the ratio $\xi_W/\xi_S > \lambda$. This unexpected result can be interpreted in the following manner: when the sulfonate concentration approaches the percolation threshold for head-groups, a fraction of the sulfonates are randomly distributed between the existing multiplets. These bridging sulfonates cannot retain their full solvation shell with λ water molecules in the hostile environment of hydrophobic backbones. The excess water molecules stripped from these 'bulk' sulfonates are consequently redistributed between the existing multiplets. This leads to the formation of an outer solvent shell around each multiplet.

D. Swelling-induced ionomer deformation

The polymer backbone and sidechains sustain conformational changes when the membrane swells. Two different types of deformation, an elongation (stretching) deformation and a coiling (frustration) deformation of polymer chains can be conveniently resolved using the probability distribution $P(\alpha)$ of the dihedral angle along the polymer chains.

The probability distribution $P(\alpha)$ of the dihedral angle along the sidechain is shown in Figure 8 for the membrane η_1. The sidechains have two *gauche* (± 82 degrees) and one *trans* conformations. When the membrane absorbs water, the sidechains undergo a deformation in which a part of the *gauche* conformations transform into *trans* conformations. The overall effect of this structural deformation is a structural relaxation of the sidechains, perceived as a stretching – an impact schematically illustrated in Figure 9. We have also detected a similar stretching-like structural relaxation for the backbone segments. As seen from Figure 10, the probabilities of the two *gauche* (± 125 degrees) and single *cis* (± 0 degrees) backbone conformations in the solvated membrane diminish when the hydration parameter λ decreases.

The extent of sidechain relaxation sensitively depends on the sulfonate concentration η. In Figure 11 we compare the $P(\alpha)$ curves for the two membranes. It is noticeable that the sidechains are in a more relaxed state in the membrane η_1 compared to the membrane η_2. This is a direct consequence of the fact that the smaller number of head groups inside the multiplet provide a more relaxed configuration for sidechains compared to the case when a larger number of sulfonates are immersed into a smaller multiplet. The dihedral frustration

of sidechains in the high-sulfonate membrane is schematically illustrated in Figure 12. A similar dihedral frustration has also been detected for the backbone polymer: in the high-sulfonate membrane the backbone segments adopt a more curly conformation.

E. Proton Diffusion

The proton mobility in solvated ionomers is strongly affected by proton–head group association effects. On the one hand, this association localizes the protons near the head groups, and therefore decreases the rate of vehicular diffusion across the membrane. On the other hand, the localization effect increases the rate of the hopping diffusion of protons from sulfonate to sulfonate. This so-called surface diffusion is believed to be additionally enhanced by the water–proton electrostatic interactions and the side-chain thermal fluctuations. The strength of the proton–sulfonate association is commonly evaluated in the terms of the proton distribution around the head-groups. Our simulation results for the sulfur-proton pair correlation function $g_{SH}(r)$ are plotted in Figure 13. The first proton shell, seen as a very high peak on the left side of Figure 13, originates from the attractive Coulomb forces between the protons and the SO_3^- groups. The second peak of $g_{SH}(r)$ on the right side of Figure 13 arises from the proton shells of neighboring sulfonates in the multiplet. The condensation effect of protons on the sulfonates is noticeably stronger in the membrane η_1 than in the case of the membrane η_2. As a consequence, the proton mobility in the membrane η_2 will be higher.

The effect of a proton–sulfonate association also depends on the membrane hydration level λ [50]: the association is weak for the hydrated membrane with $\lambda = 1$, whereas it is strong for the membrane with $\lambda = 5$. The position of the minimum of $g_{SH}(r)$ corresponds to the position of the first maximum of $g_{SS}(r)$ in Figure 4.

The mean square displacements (msd) of protons for different membrane hydrations λ are plotted in Figure 14. As is expected from the proton delocalization effect in hydrated membranes, higher membrane hydrations result in larger proton displacements [49]. The msd result for the membrane η_1 is below the corresponding result for the membrane η_2 for Run 4. This happens partly due to the strong proton delocalization effect, and partly due to the small nearest-neighbor distances R_B^S in the membrane η_2.

The calculated values for the diffusion coefficient of protons,

$$D = \lim_{t \to \infty} \frac{\text{msd}(t)}{6t} \ , \tag{11}$$

are gathered in Table III. The proton diffusion, similar to the proton mobility, is stronger in membrane η_2 than in membrane η_1 because of the low proton-sulfonate association. There are two other factors that contribute to the proton diffusion of membrane η_2: the existence of 'bulk' sulfonates between neighboring multiplets and the accumulation of water molecules around the multiplets. Both these factors can lead to the formation of temporary bridges, sulfonic and/or solvent in nature, between the multiplets. Our results for proton diffusion are in good agreement with the simulation results of Ref. [49]. However they are small compared to the proton diffusion coefficients experimentally observed in fully hydrated Nafion ionomers. This discrepancy is most probably not due to our neglect of the Grotthuss mechanism, which is strongly suppressed when λ is small [56, 57, 58], but is a consequence of the reduced number of pathways in our low-humidity, low-sulfonate model.

V. DISCUSSION

We have investigated the swelling properties of multiplets in low humidity ionomers with low sulfonate concentration by examining different models for the sidechain architecture. Our primary goal was to determine the dependence of multiplet swelling on the hydration level λ and the sulfonate concentration η of the membrane.

Our main result is the fission of the sulfonate multiplets into smaller parts at the onset of membrane hydration. This behavior is not explained by the classical theories of cluster swelling in ionomers, according to which the swelling should be a continuous and monotonic process of multiplet expansion. The resultant small multiplets will consequently swell, keeping the number of their sulfonate population constant, when more water is absorbed into the membrane. We have also found that the location of the of water in low-sulfonate membranes strongly depends on the sulfonate concentration. For a relatively low sulfonate concentration nearly all sulfonate groups are in multiplet formations. The average water loading parameter per multiplet χ_W/χ_S, where χ_W is the number of water molecules belonging to the multiplet, and χ_S is the number of sulfonates in the multiplet, perfectly matches the water content of the membrane λ. However, for relatively high sulfonate concentrations, the

15

water loading parameter per multiplet χ_W/χ_S is consistently larger than the parameter λ for the membrane hydration levels considered. We assume that, when the sulfonate concentration approaches the percolation threshold for head-groups, a fraction of the sulfonates are randomly distributed between the existing multiplets. These bridging sulfonates cannot retain their full solvation shell in the hostile environment of hydrophobic backbones. The excess water molecules stripped from these 'bulk' sulfonates are consequently redistributed between the existing multiplets. The results of our structural analysis confirm the formation of unexpected water shells around sulfonate multiplets. The multiplet fission and the water encapsulation effects are illustrated schematically in Figure 15.

Our discovery of the uneven distribution of the water-to-sulfonate loading in the ionomer opens a new window into the percolation characteristics of the hydrophilic network in ionomers. It is no longer sufficient to have a continuous pathway among sulfonates in order for percolation of protons to occur, as some of these sulfonates may be found in the hydrophobic material, where they are not capable of contributing to proton transport. The predicted hydration levels necessary for good transport of protons will thus be higher than they would be if the presence of sulfonates encapsulated in backbone material were ignored.

We have also analyzed the structural deformations occurring in the ionomer as a result of membrane swelling, and found that in swollen membranes the ionomer is in a more relaxed state. The degree of relaxation, however, is sensitive to the sulfonate concentration: the sidechains and backbones are found to be more relaxed in low-sulfonate membranes. This result is a direct consequence of the fact that in low-sulfonate membranes the sulfonate cluster is less dense, and can relax more readily than in the denser environment of the high-sulfonate material. However, proton diffusion is stronger in high-sulfonate membranes, and can potentially benefit from the formation of temporary solvent and sulfonate bridges between the multiplets.

An interesting question, yet to be resolved, is whether the multiplet splitting and shrinking effects depend on the pretreatment history of the membrane. The membrane morphology is known to be affected by the type of pretreatment, such as boiling, annealing, drying, poling, stretching, etc., and by the order in which these steps are taken. In most cases the impact of the pretreatment is either the formation of a new morphology with an anisotropy in the backbone and sidechain orientations, or the reshaping of the network of hydrophilic clusters. In our current work the dry membrane was 'numerically pretreated' by our frag-

mentation and de-fragmentation procedures, as described in section III. We assume that our membrane has a network of hydrophilic pores resembling the network in a mold-extruded membrane, provided it has then been annealed.

In order to analyze the consequences of the residual anisotropy in the ionomer on the multiplet reorganization effects reported in this work, we carried out test simulations for a poled and dry Nafion-like ionomer. According to our previous results on ionomer poling [33], rod-like aggregations of head groups are formed along the direction of the applied electric field. The poled structures were found to be stable after the release of the poling field. One of the poled structures of Ref. [33] was used as a starting configuration for Run 1 of our current work. Our simulation result indicated that a similar reorganization effect of sulfonate multiplets, as seen in the case of isotropic membranes, takes place. Hence, we conclude that the splitting and shrinking effects are robust against structural anisotropy in the membrane.

We also performed test simulations to clarify the nature of multiplet reorganization in dry membranes that had been previously swollen. The hydrated membrane from Run 4 with water content $\lambda=5$ was first dried through a simple elimination of all water molecules in the simulation box. Then the water-free membrane was gradually shrunk to the system size used for Run 1. The results obtained show that the initially dry membrane, membrane I, and the pretreated dry membrane, membrane II, have different structures. In the latter the multiplet sizes R_A^S were smaller and close to the multiplet sizes corresponding to Run 2. However, after annealing at high temperatures, the discrepancies between the membranes disappeared, and both membranes exhibited the splitting and shrinking of multiplets at the onset of hydration.

In future work, we plan to extend the model presented here to take into account the partial charges on the side-chain monomers. Our preliminary results indicate that a partial delocalization of the negative charge along the sidechain head group has a noticeable role in the membrane swelling process.

Table I: List of key variables.

λ	number of water molecules per sulfonate group
σ	monomer diameter
ϵ	dielectric constant of medium
Q_p, Q_S, Q_{O_3}	normalized charges of protons, sulfur atoms and head group oxygens
ε_{LJ}	Lennard-Jones interaction parameter between monomers
k_b, k_θ, k_α	stretching, bending and torsion force constants
r_0	equilibrium bond length for backbone and sidechain
θ_0	equilibrium bending angle for backbone and sidechain
k_B, T	Boltzmann constant and system temperature
n_1, n_2	number of hydrophobic and hydrophilic monomers per sidechain
n_3	number of hydrophobic backbone monomers between adjacent sidechains
η	molar concentration of head groups
N_0	Avogadro's number
N, N_S	total number of ionomer monomers, number of sulfonates
L, V	length of simulation box, volume of simulation box
$g_{SS}(r), g_{SH}(r)$	sulfonate-sulfonate and sulfonate-proton pair correlation functions
$g_{WW}(r)$	water-water pair correlation function
R_A^S, R_A^W	size of sulfonate-sulfonate multiplets and water clusters
R_B^S, R_B^W	nearest-neighbor distance between for sulfonate multiplets and water clusters
χ_S, χ_W	number of head groups and number of water molecules in a multiplet
ξ	number of multiplets in the simulation box
l_D	electrostatic screening length
$\bar{l}$	average separation distance between sulfonates
$S(q), q = 2\pi/r$	sulfonate-sulfonate structure factor
$\overline{R}$	correlation length of density-density fluctuations of sulfonates
$P(\alpha)$	Probability distribution of the dihedral angle along the polymer segments
D	diffusion coefficient of protons
ρ	3D density of membrane components

Table II: Parameters used in simulation runs. Here $n_1 + n_2$ is the total number of monomers per sidechain, λ is the water content per head group.

Runs	hydration model	$n_1 + n_2$
Run 1	dry ionomer with no water, λ=0	10
Run 2	ionomer with explicit water, λ=1	9
Run 3	ionomer with explicit water, λ=3	9
Run 4	ionomer with explicit water, λ=5	9

Table III: Calculated ionomer parameters for membranes with sulfonic molar concentration η_1 and η_2 (shortly called membranes η_1 and η_2 in the text. The definitions of the parameters used are given in Table I.

				membrane η_1					
λ	R_A^S	R_B^S	$\overline{R}$	R_A^W	R_B^W	χ_S	χ_W	χ_W/χ_S	$D(\text{cm}^2/\text{sec})$
0	5.3	9.6	10	−	−	16	−	−	−
1	4.7	7.9	7.5	4.7	7.9	10	10	1	2.7×10^{-6}
3	4.9	8.1	7.7	4.9	8.1	10	30	3	4.5×10^{-6}
5	5.0	8.5	8.0	5.0	8.5	10	50	5	5.2×10^{-6}

				membrane η_2					
λ	R_A^S	R_B^S	$\overline{R}$	R_A^W	R_B^W	χ_S	χ_W	χ_W/χ_S	$D(\text{cm}^2/\text{sec})$
0	5.0	9.4	9.97	−	−	22	−	−	−
1	4.2	7.9	7.64	4.8	7.7	13	17	1.2	3.5×10^{-6}
3	4.4	8.0	8.0	5.1	8.04	13	62	4.5	5.2×10^{-6}
5	4.6	8.2	8.35	5.2	8.32	13	101	7.8	6.5×10^{-6}

[1] McAlevy, U.S. Patent 2,405,971 (August 29, 1946).

[2] M. I. Perry, T. F. Fuller, J. Electrochemical Society **149**, S59 (2002).

[3] A. Sacca, A. Carbone, R. Pedicini, G. Portale, L. D'Ilaro, A. Longo, A. Martorana, E. Passalacqua, J. Membrane Science **278**, 105 (2006).

[4] M. Saito, K. Hayamizu, T. Okada, Phys. Chem. B, **109**, 3112 (2005).

[5] K. D. Kreuer, Journal of Membrane Science **185**, 29 (2001).

[6] B. Smitha, S. Sridnar, A. A. Khan, J. Polym Sci: part B: Polymer. Phys. **43**, 1538 (2005).

[7] D. J. Connolly, W. F. Gresham, U.S. Patent 3,282,875 DuPont Co. (November 1, 1966); D. A. Hounshell, J. K. Smith Jr., Science and Corporate Strategy- DuPont R&D, 1902-1980, Cambridge University Press, Cambridge, UK (1988).

[8] S. Banerjee, D. E. Curtin, J. Fluorine Chemistry **125**, 1211 (2004).

[9] W. Y. Hsu, T. D. Gierke, Macromolecules **15**, 101 (1982); *ibid* J. Memb. Sci. **13**, 307 (1982); T. D. Gierke, G. E. Munn, F. C. Wilson, J. Polym. Sci. Phys. Ed. **19**, 1687 (1981).

[10] M. A. F. Robertson, Ph.D. Thesis, University of Calgary (1994).

[11] N. H. Jalani, Ph.D. Thesis, Worcester Polytechnic Institute (2006).

[12] K. A. Mauritz, C. J. Hora, A. J. Hopfinger, Polym. Prepr. (Am. Chem. Soc. Div. Polym. Chem.), **19**, 324 (1978); K. A. Mauritz, C. E. Rogers, Macromolecules **18**, 483 (1985).

[13] K. A. Mauritz, R. B. Moore, Chem. Rev. **104**, 4535 (2004).

[14] H. L. Yeager, A. Steck, J. Electrochem. Soc. **128**, 1880 (1981).

[15] A. Eisenberg, Macromolecules **3**, 147 (1970); Macromolecules **30**, 7914 (1997).

[16] M. H. Litt, Polymer Preprints **38**, 80 (1997).

[17] G. Gebel, O. Diat, Fuel Cells **5**, 261 (2005); L. Rubatat, O. Diat, G. Gebel, Physical Chemistry and Soft Matter **106**, 1 (2004).

[18] K. Schmidt-Rohr, Q. Chen, Nat. Mater. **7**, 75 (2008).

[19] Paddison, S. J.; Reagor, D. W.; Zawodzinski, T. A. J. Electroanalyt. Chem. **91**, 459 (1998).

[20] S. Slade, S. A. Campbell, T. R. Ralph, F. C. Walsh, J. Electrochem. Soc. **149**, A1556 (2002).

[21] M. Cappadonia, J. W. Erning, U. Stimming, J. Electroanalyt. Chem. **376**, 189 (1994).

[22] H.-L. Lin, T. L. Yu, F.-H. Han, J. Polym. Research **13**, 379 (2006).

[23] H.-L. Lin, T. L. Yu, C.-H. Huang, T.-L. Lin, J. Polymer Science B: Polymer Physics **43**, 3044

(2005).

[24] V. Arcella, C. Trogila, A. Ghielmi, Ind. Eng. Chem. Res. **44**, 7646 (2005).

[25] Y. Yamamotoa, M. C. Ferrari, M. Giacinti, M. G. Baschetti, M. G. De Angelis, G. C. Sarti, Desalination **200**, 636 (2006).

[26] J. Fimrite, H. Struchtrup, N. Djilali, J. Electrochemical Society **152**, A1804 (2005).

[27] M. Laporta, M. Pegoraro, L. Zanderighi, Phys. Chem. Chem. Phys. **1**, 4619 (1999).

[28] S. Lue, S. J. Shieh, J. Macromol. Sci.B: Physics **48**, 114 (2009).

[29] S. Dokmaisrijan, E. Spohr, J. Mol. Liquids **129**, 92 (2006).

[30] J. T. Wescott, Y. Qi, L. Subramanian, T. W. Capehart, J. Chem. Phys. **124**, 134702 (2006).

[31] A. Vishnyakov, A. V. Neimark, Mesoscale Simulations of Hydrated Nafion Membranes, AICHE Annual Meeting, San Francisco (2006).

[32] E. Allahyarov, P. Taylor, J. Chem. Phys. **127**, 154901 (2007).

[33] E. Allahyarov, P. Taylor, Phys. Rev. E **80**, 020801(R) (2009).

[34] A. Vishnyakov, A. V. Neimark, J. Phys. Chem. B **105**, 7830 (2001); *ibid* 9586 (2001).

[35] E. Allahyarov, P. Taylor, J. Phys. Chem. B **113**, 610 (2009).

[36] Z. Lu, G. Polizos, D. D. Macdonald, E. Manias, J. Electrochem. Soc. **155**, B163 (2008).

[37] C. G. Vayenas, M. N. Tsampas, A. Katsaounis, Electrochimica Acta **52**, 2244 (2007).

[38] S. J. Paddison, T. A. Zawodzinski, Solid State Ionics **113-115**, 333 (1998).

[39] S. J. Paddison, Annu. Rev. Mater. Res. **33**, 289 (2003).

[40] G. Gebel, R. B. Moore, Macromolecules **33**, 4850 (2000).

[41] S. J. Paddison, J. A. Elliott, J. Phys. Chem. **109**, 7583 (2005).

[42] K. Chan, Y. W. Tang, I. Szalai, Molecular Simulations **30**, 81 (2004).

[43] S. S. Jang, V. Molinero, T. Cagin, W. A. Goddard III, J. Phys. Chem. B, **108**, 3149 (2004).

[44] A temporary fragmentation of ionomer molecules into smaller segments in order to speed up its equlibration in molecular dynamics simulations is equivalent of heating up the ionomer above its glass transition temperature T_g in experiments.

[45] A. Vishnyakov, A. V. Neimark, J. Phys. Chem. B **104**, 4471 (2000).

[46] D. Rivin, G. Meermeier, N. S. Schneider, A. Vishnyakov, A. V. Neimark, J. Phys. Chem. B **108**, 8900 (2004).

[47] J. A. Elliott, S. Hanna, A. M. S. Elliott, G. E. Cooley, Phys. Chem. Chem. Phys. **1**, 4855 (1999).

[48] M. Mazars, J. Chem. Phys. **115**, 2955 (2001).

[49] S. Cui, J. Liu, M. E. Selvan, D. J. Keffer, B. J. Edwards, W. V. Steele, J. Phys. Chem. B **111**, 2208 (2007).

[50] S. Cui, J. Liu, M. E. Selvan, S. J. Paddison, D. J. Keffer, B. J. Edwards, J. Phys. Chem. B **112**, 13273 (2008).

[51] G. Brunello, S. G. Lee, S. S. Jang, Y. Qi, J. Renewable and Sustainable Energy **1**, 033101 (2009).

[52] E. Spohr, Mol. Simul. **30**, 107 (2004).

[53] J. A. Elliott, S. Hanna, A. M. S. Elliott, G. E. Cooley, Polymer Engineering and Science **46**, 228 (2006).

[54] S. K. Young, S. F. Trevino, N. C. Tan, J. Polymer Science: Part B, Polymer Physics **40**, 387 (2002).

[55] P. Choi, N. H. Jalani, R. Datta, J. Electrochemical Society **152**, E123 (2005).

[56] D. Seeliger, C. Hartnig, E. Spohr, Electrochim Acta **50**, 4234 (2005).

[57] M. Eikerling, A. A. Kornyshev, U. Stimming, J. Phys. Chem. **101**, 10807 (1997).

[58] E. L. Thompson, T. W. Capehart, T. J. Fuller, J. Jorne, J. Electrochem. Society **153**, A2351 (2006).
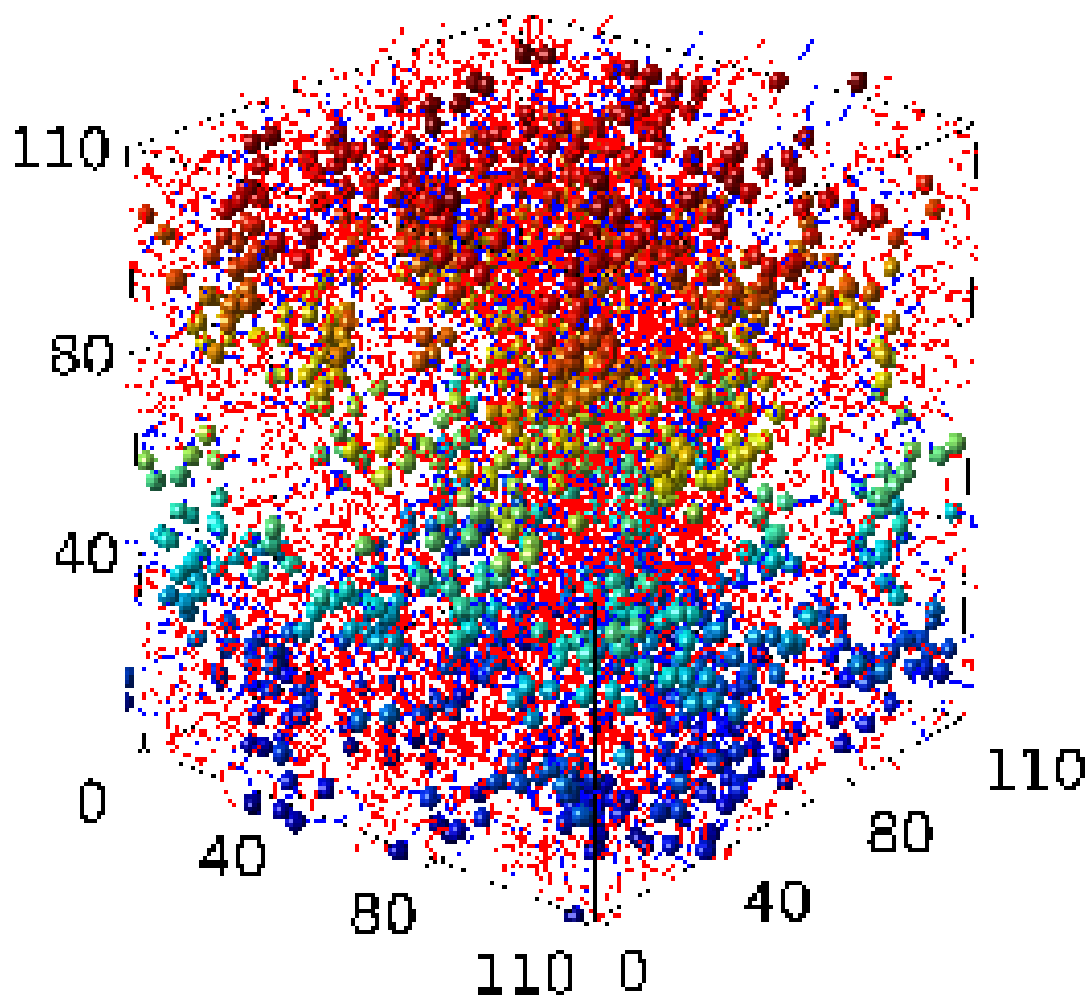
Figure 1: (Color online) A typical snapshot of hydrated membrane η_2 from Run 3. The spheres represent the end-group oxygens of the sidechains. The polymer is shown by red lines. Different bead colors correspond to different bead altitudes, with a blue color for low-altitude beads (at the bottom of simulation box) and a red color for high-altitude beads (at the top of simulation box). The size of all structural elements is schematic rather than space filling. The water molecules and protons are not shown for the sake of clarity.
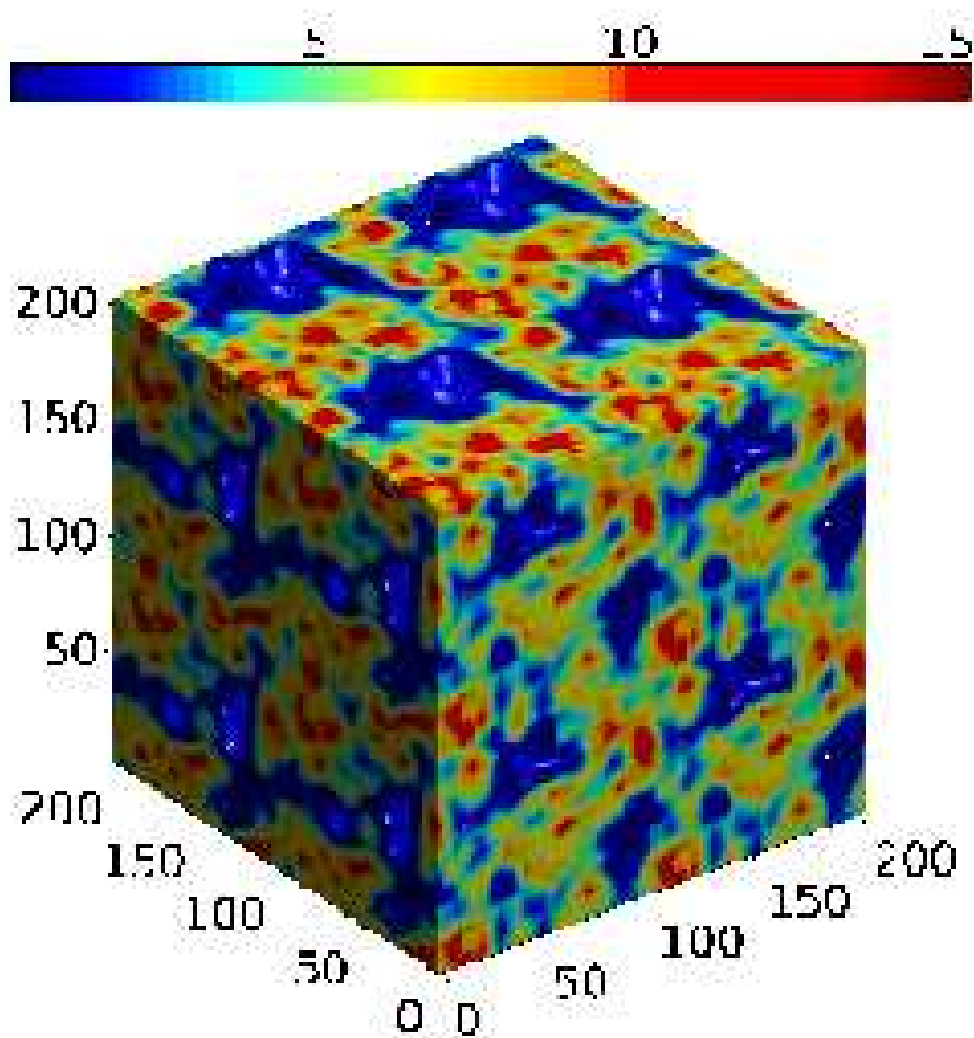
Figure 2: (Color online) 3D density $\rho(\vec{r})$ of the hydrophobic part of the membrane η_2 for Run 3. The color gradient from dark blue (black in printed version) to dark red (gray in printed version), corresponds to the variation of membrane density from low to high values. The axis dimension is in Å.
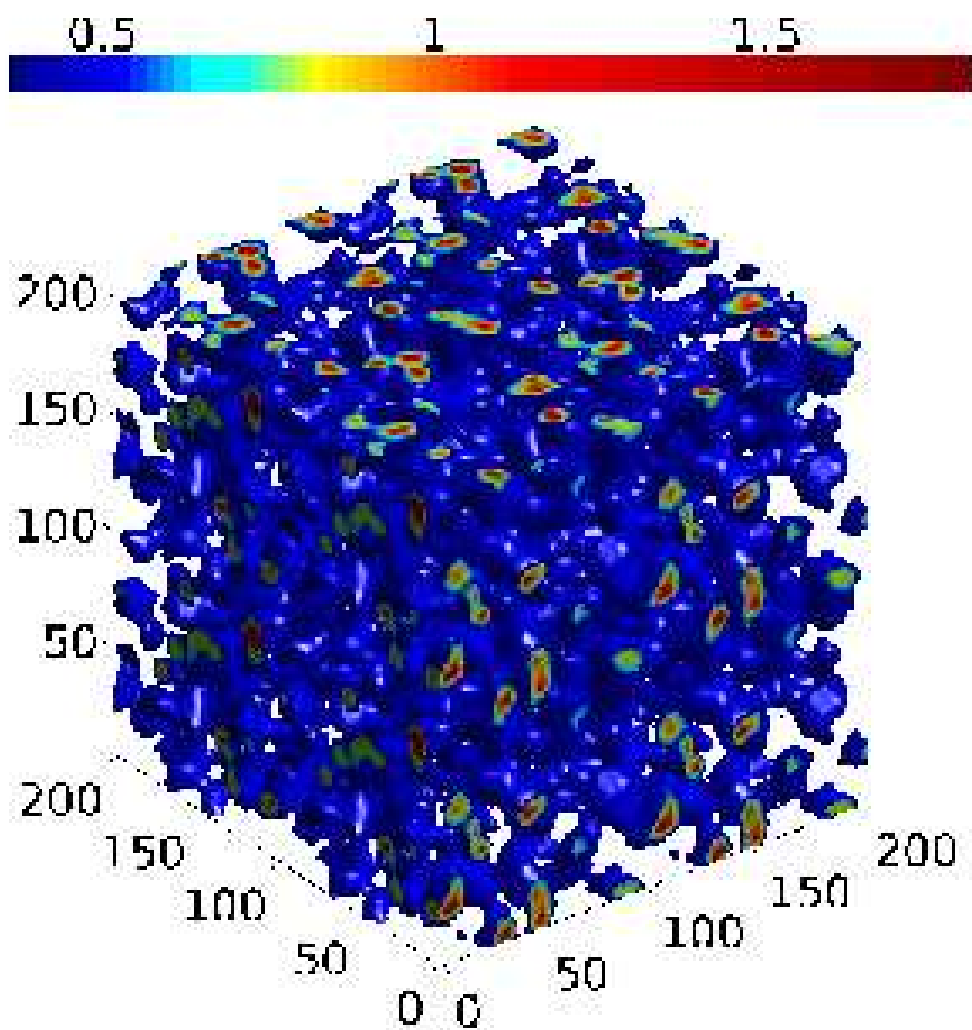
Figure 3: (Color online) 3D density of water channels for the membrane η_2 and Run 3. The color gradient from dark blue (black in printed version) to dark red (gray in printed version) corresponds to the variation of water density from low values to high values. The axis dimension is in Å.
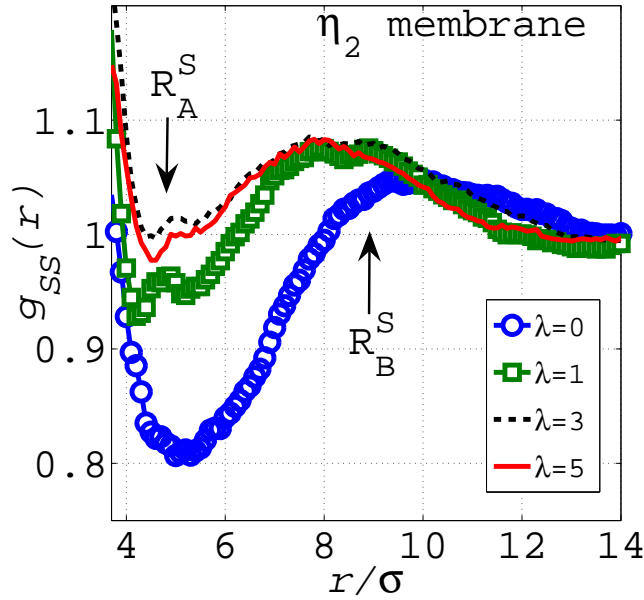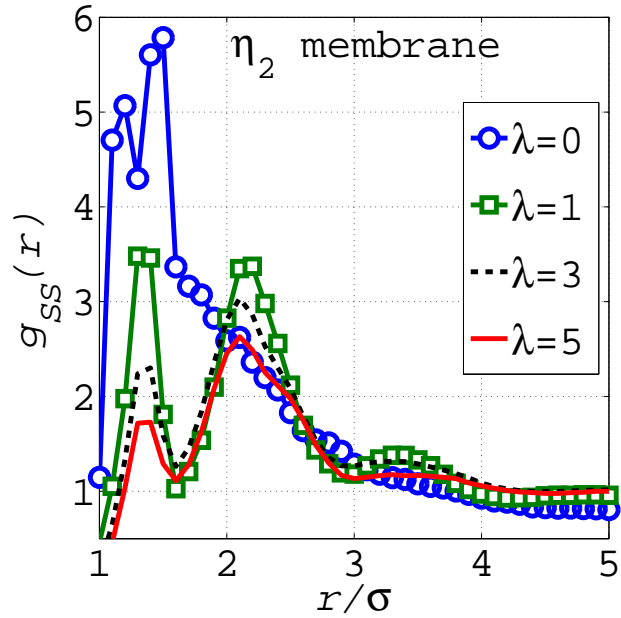
Figure 4: (Color online) Sulfonate-sulfonate pair correlation function $g_{SS}(r)$ for membrane η_2 as a function of sulfur-sulfur separation distance r for Runs 1–4 from Table II. Solid line with circles - Run 1, solid lines with squares- Run 2, dashed line- Run 3, full line- Run 4. The bottom figure shows in detail the long-range tail of $g_{SS}(r)$ used to determine the average multiplet size R_A^S and the separation distance between the sulfonate multiplets R_B^S. The calculated values for the parameters R_A^S and R_B^S are given in Table III.
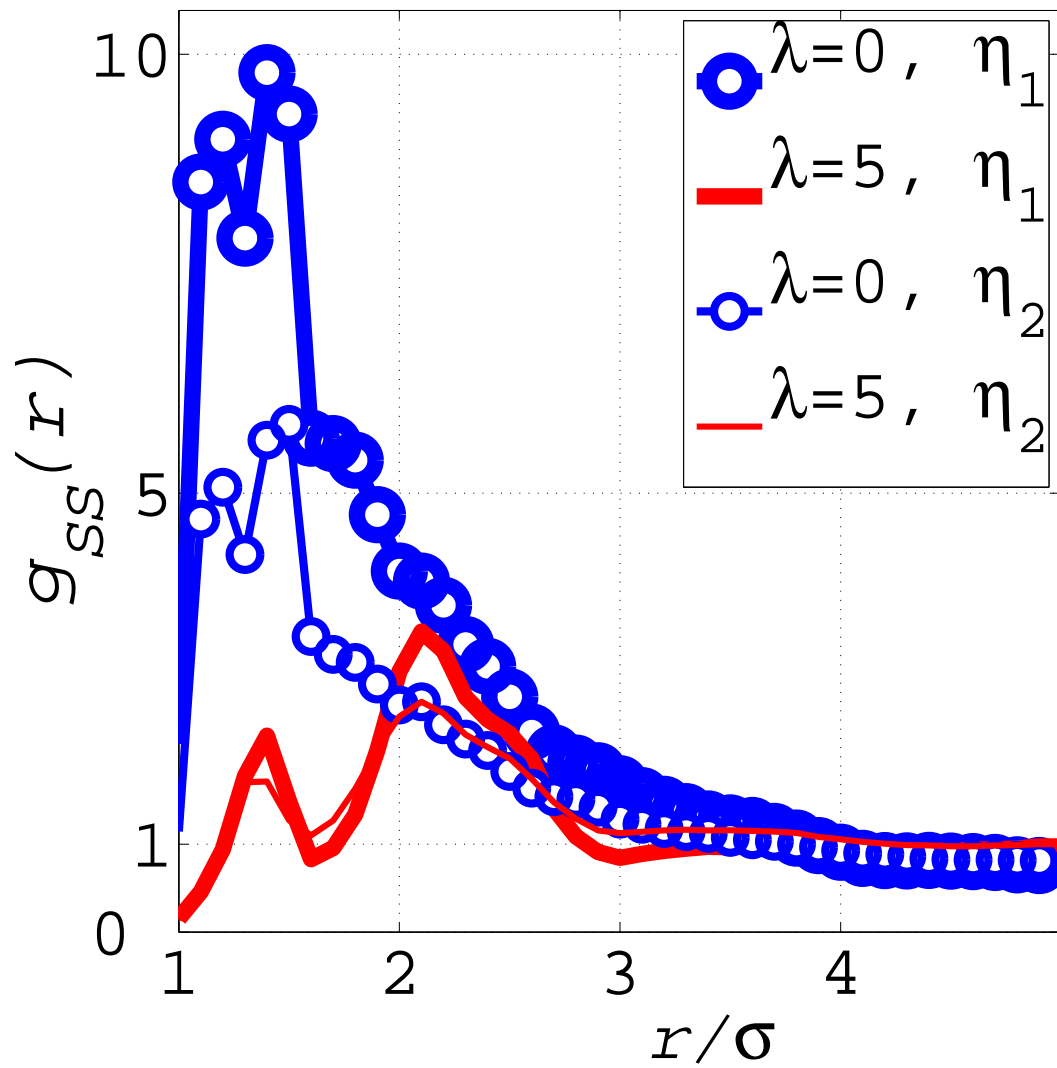
Figure 5: (Color online) Sulfonate-sulfonate pair correlation function $g_{SS}(r)$ for the membranes η_1 and η_2 as a function of the sulfur-sulfur separation distance r. Lines with symbols- Run 1, full lines- Run 4.
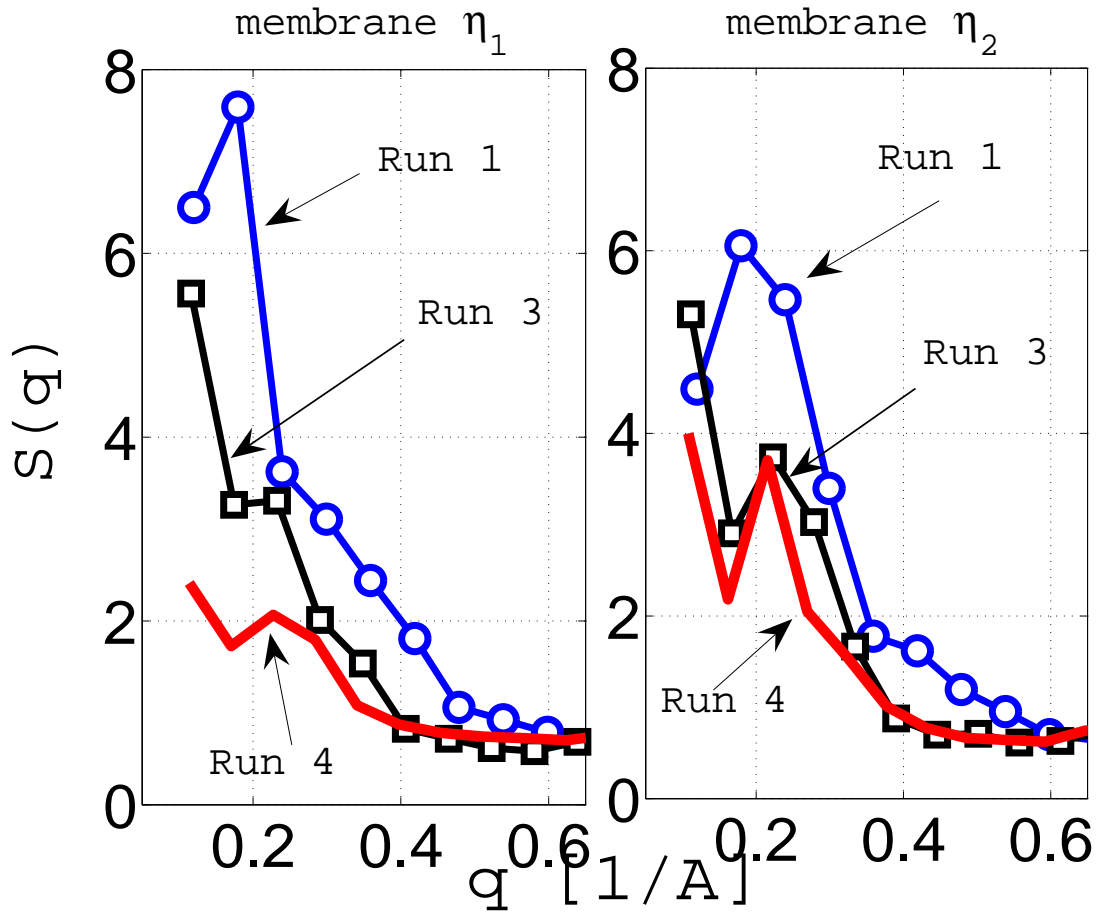
Figure 6: (Color online) Small angle ionomer peak region of sulfonate-sulfonate structure factor $S(q)$ for the membranes η_1 and η_2. Line with circles- Run 1, line with squares- Run 3, full line- Run 4. The step size $\delta q = 2\pi/L \approx 0.05\text{Å}^{-1}$ defines the resolution along the x-axis.
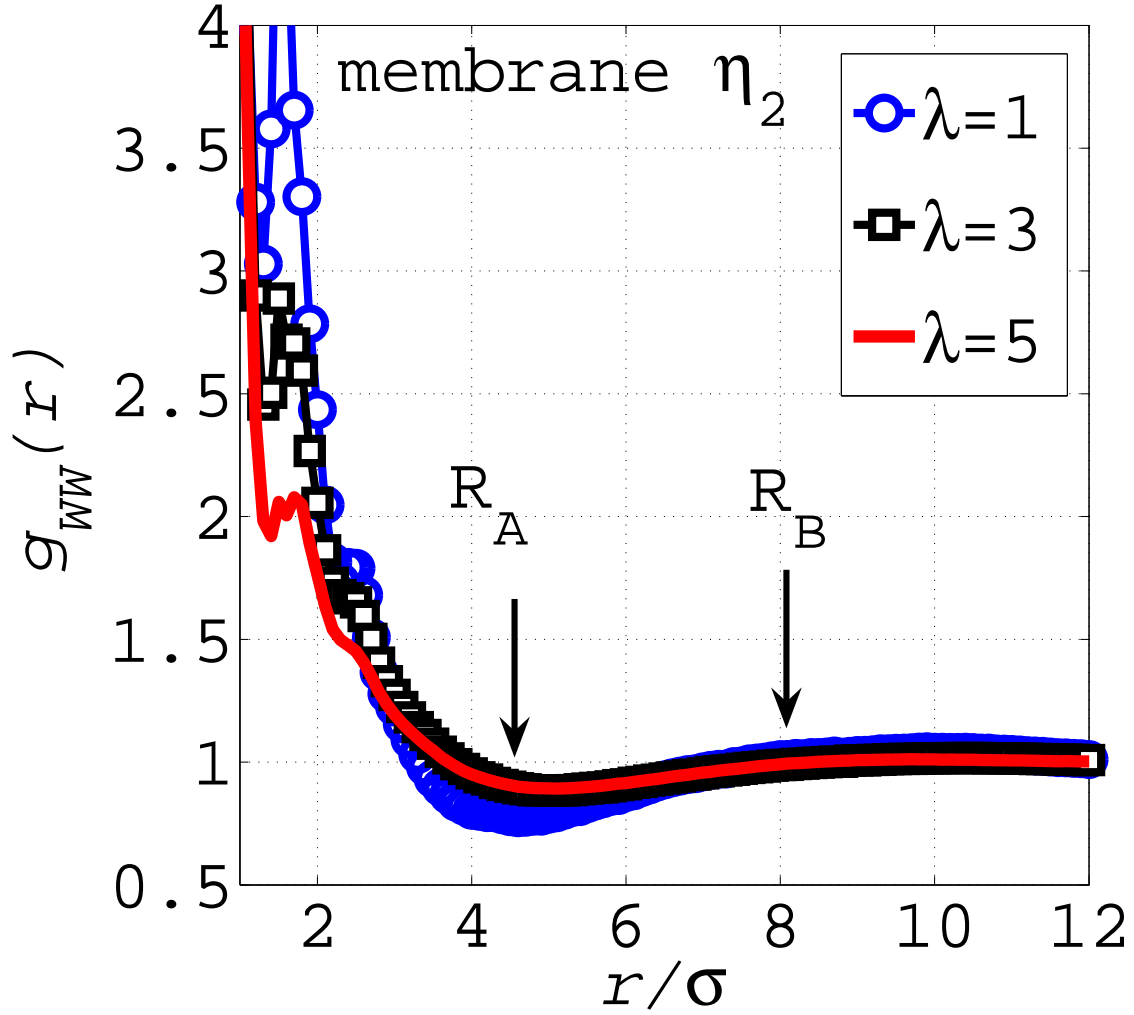
Figure 7: (Color online) Water-water pair correlation function $g_{WW}(r)$ for the membrane η_2 as a function of the water-water separation distance r for Runs 2–4 from Table II. Solid line with circles - Run 2, solid lines with squares- Run 3, full line- Run 4. The arrows show the average multiplets size R_A^W and the separation distance R_B^W between the water clusters. The calculated values for the parameters R_A^W and R_B^W are given in Table III.
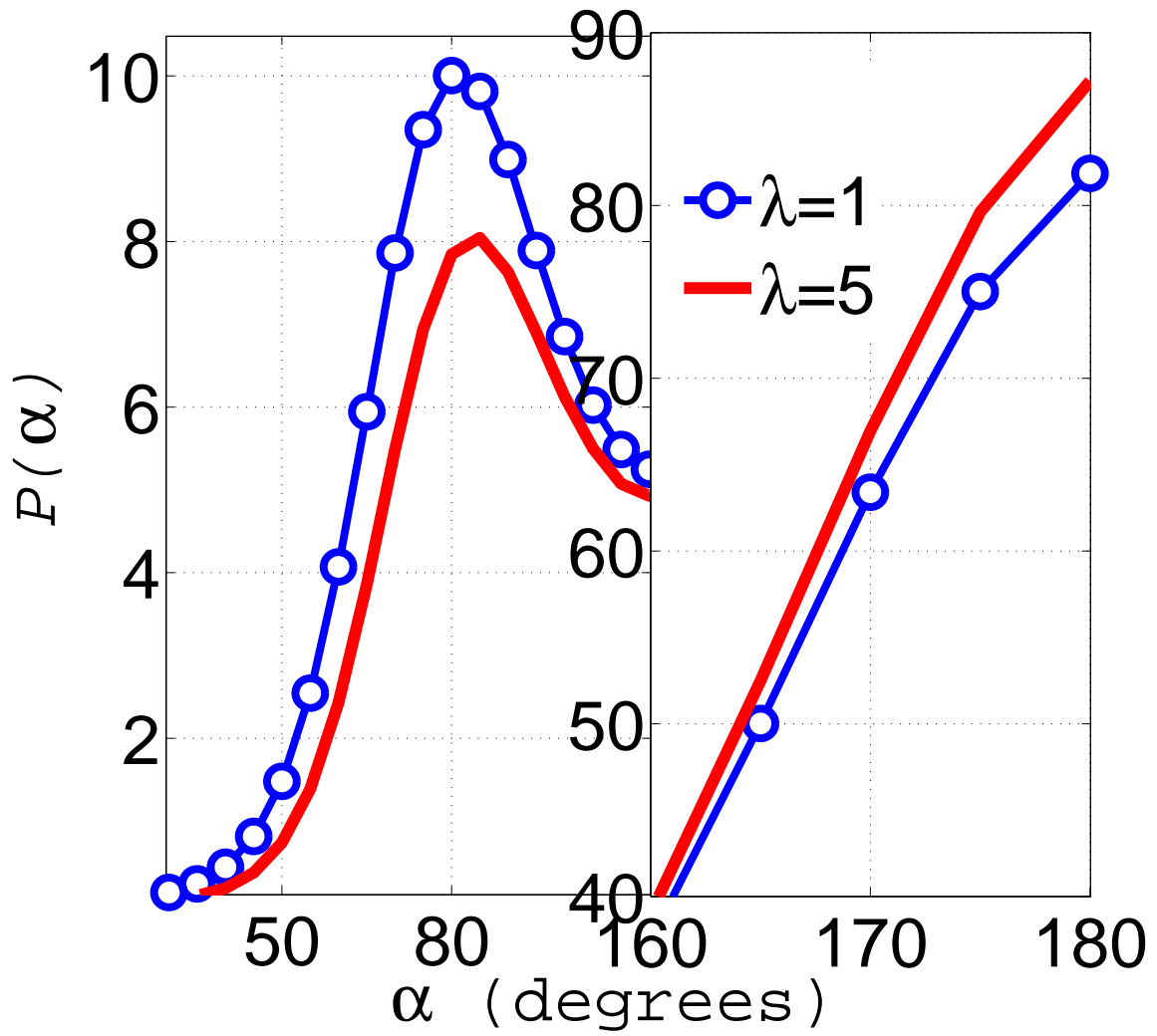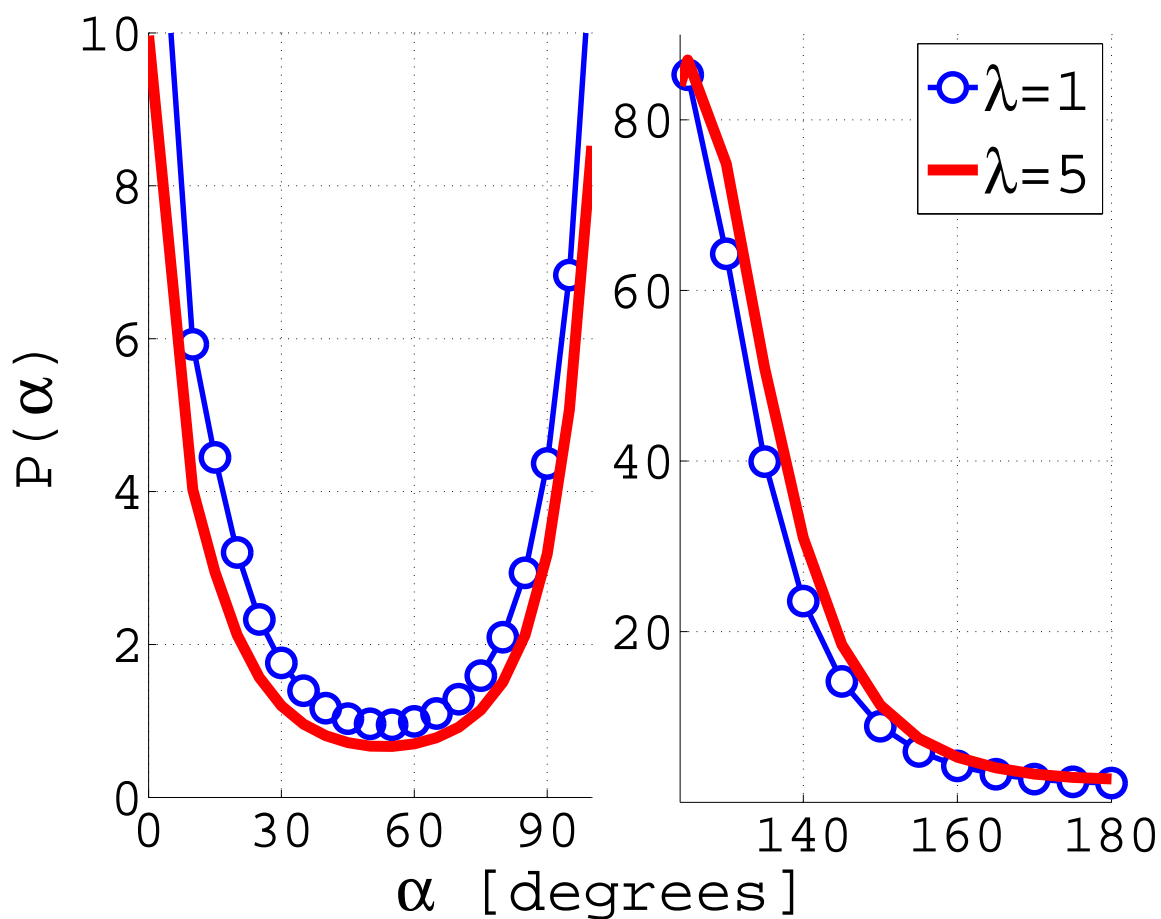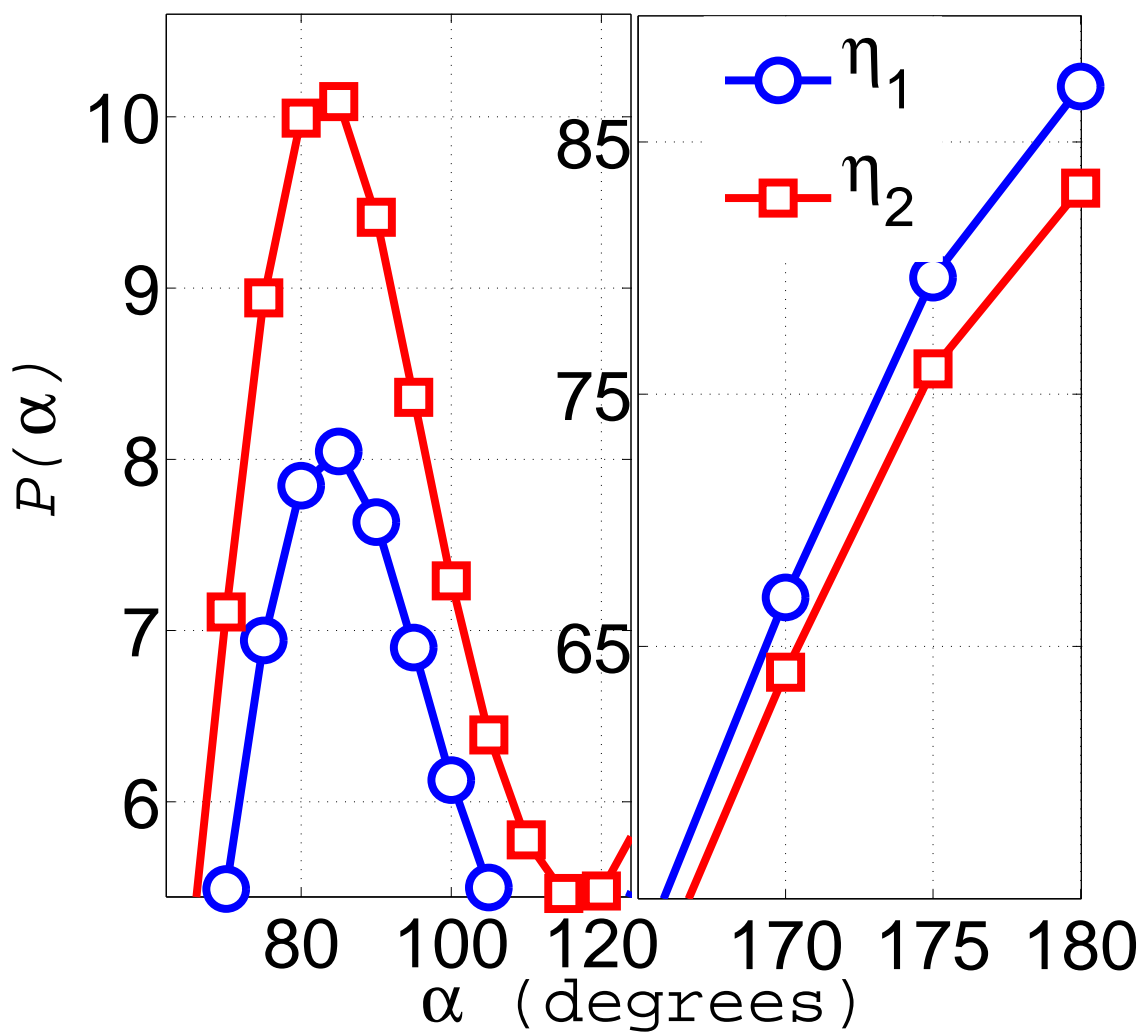
Figure 8: (Color online) The probability distribution $P(\alpha)$ of the dihedral angle along the sidechain of membrane η_1, and for Run 2 and Run 4. The areas of the *gauche* conformation ($\alpha = 82$ degrees) and the *trans* conformation ($\alpha = 180$ degrees) are shown separately.
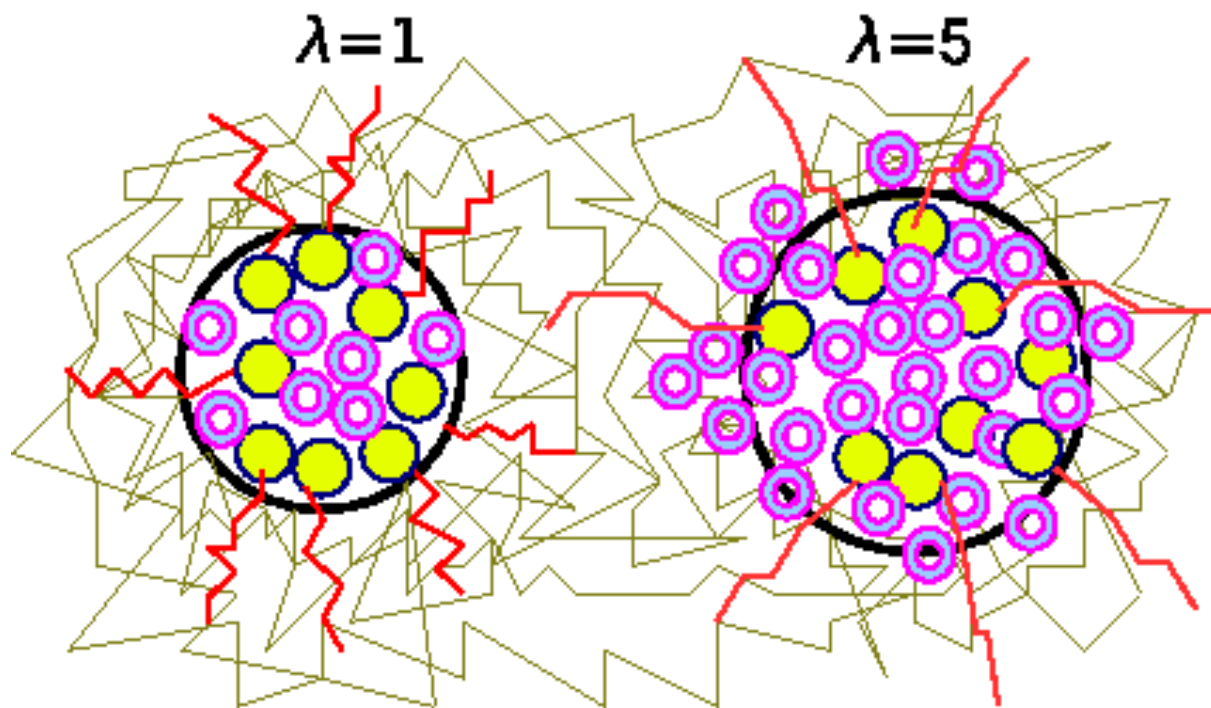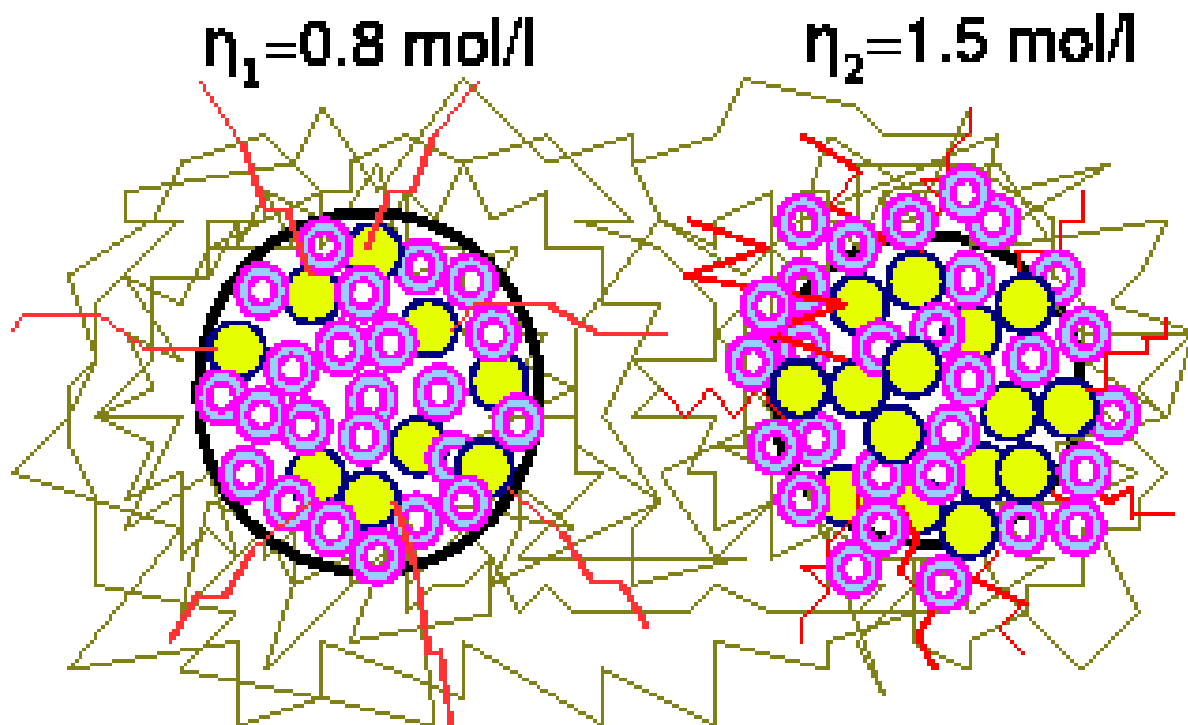
Figure 9: (Color online) Schematic pictures explaining the sidechain stretching-like relaxation as a result of multiplet swelling from $\lambda = 1$ to $\lambda = 5$. The small hollow spheres are the water molecules, gray (yellow in online version) small spheres with attached tails are for sidechains, big spheres represent the multiplets.

Figure 10: (Color online) The probability distribution $P(\alpha)$ of the dihedral angle along the backbone of membrane η_1 for Run 1 and Run 4. The areas of a *cis* conformation ($\alpha = 0$ degrees) and the *gauche* conformation ($\alpha = 125$ degrees) are shown separately.

Figure 11: (Color online) The probability distribution $P(\alpha)$ of the dihedral angle along the sidechains of membranes η_1 and η_2, and for Run 4. The areas of the *gauche* conformation ($\alpha = 82$ degrees) and the *trans* conformation ($\alpha = 180$ degrees) are shown separately.

Figure 12: (Color online) Schematic pictures explaining the differences between the stretching-like relaxation of sidechains for the membranes η_1 and η_2. The small hollow spheres are the water molecules, gray (yellow in online version) small spheres with attached tails are for sidechains, big spheres represent the multiplets.
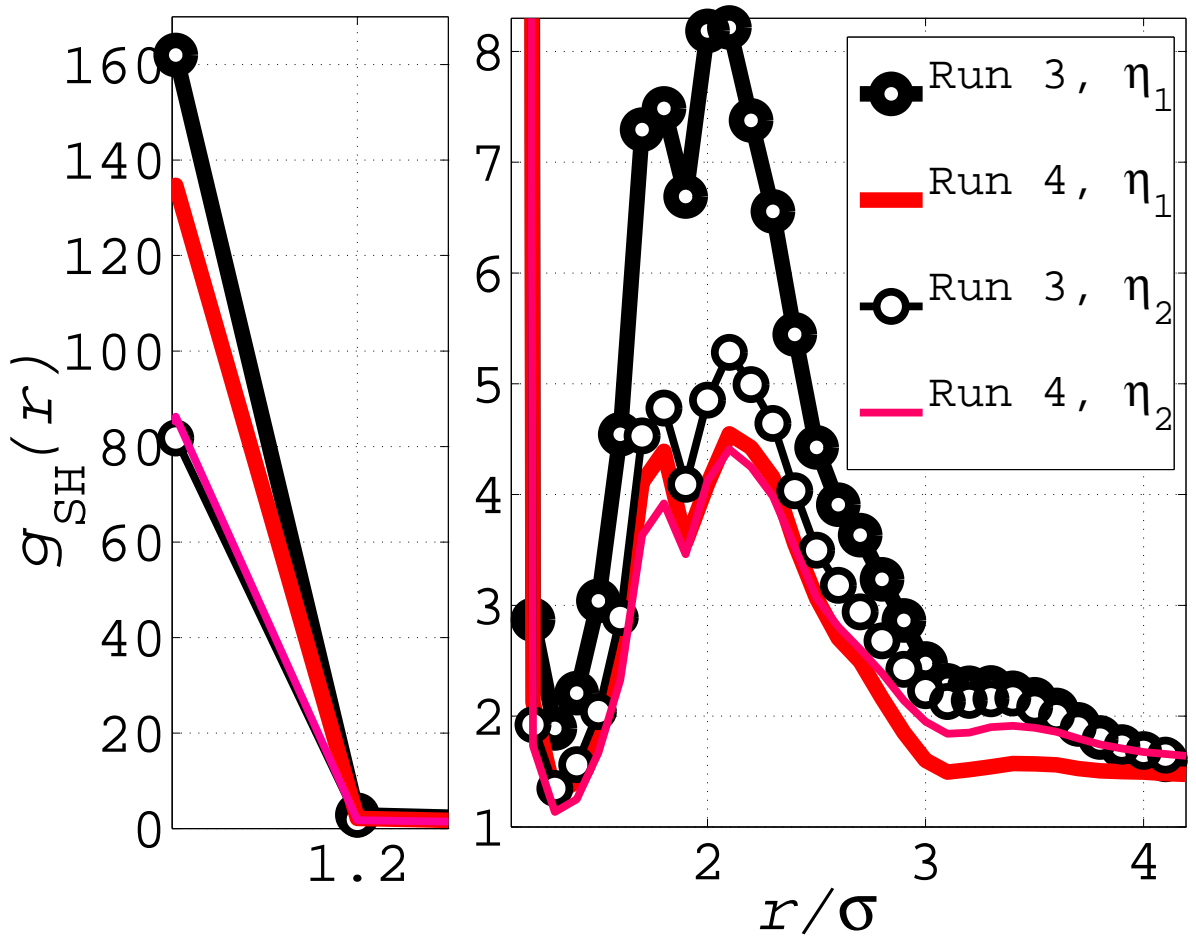
Figure 13: (Color online) Sulfonate-proton correlation function $g_{SH}(r)$ as a function of the separation distance r. The first and second peak areas are shown separately. Thick lines are for the membrane η_1, thin lines are for the membrane η_2. Line with symbols- Run 3, full lines- Run 4.
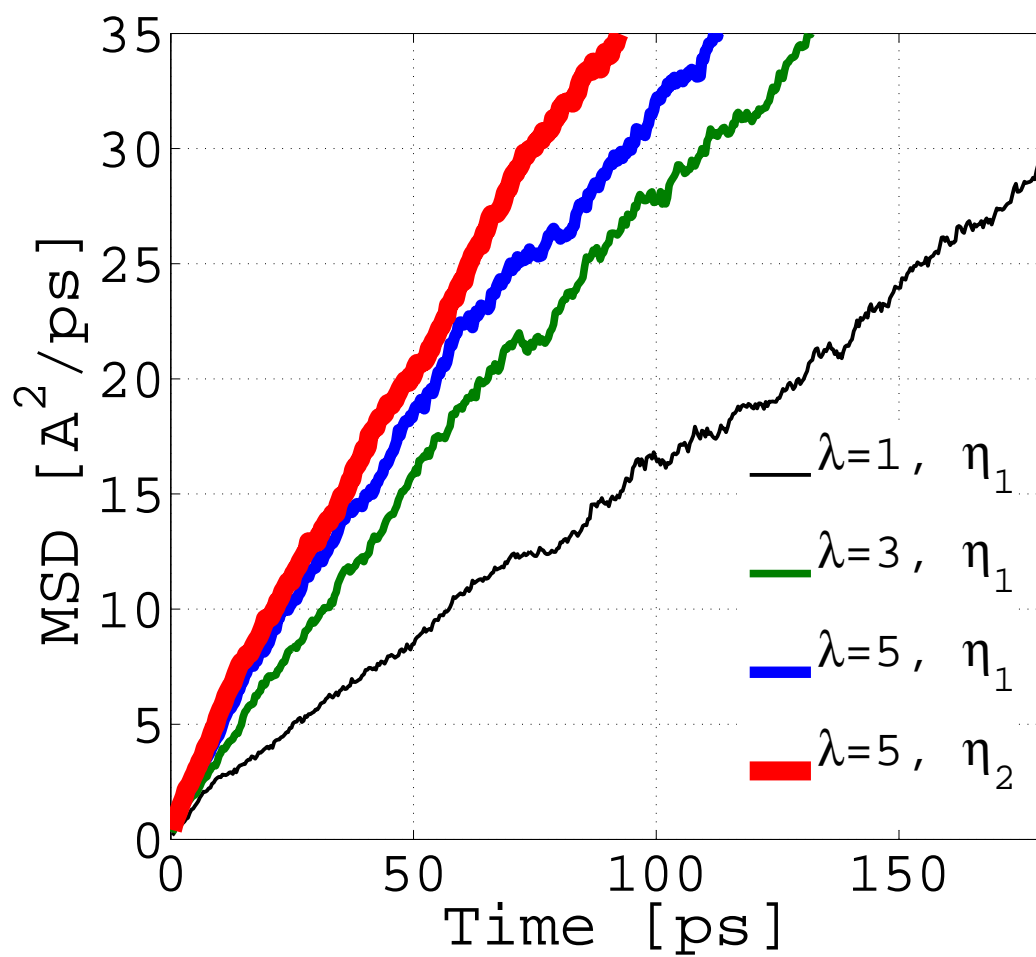
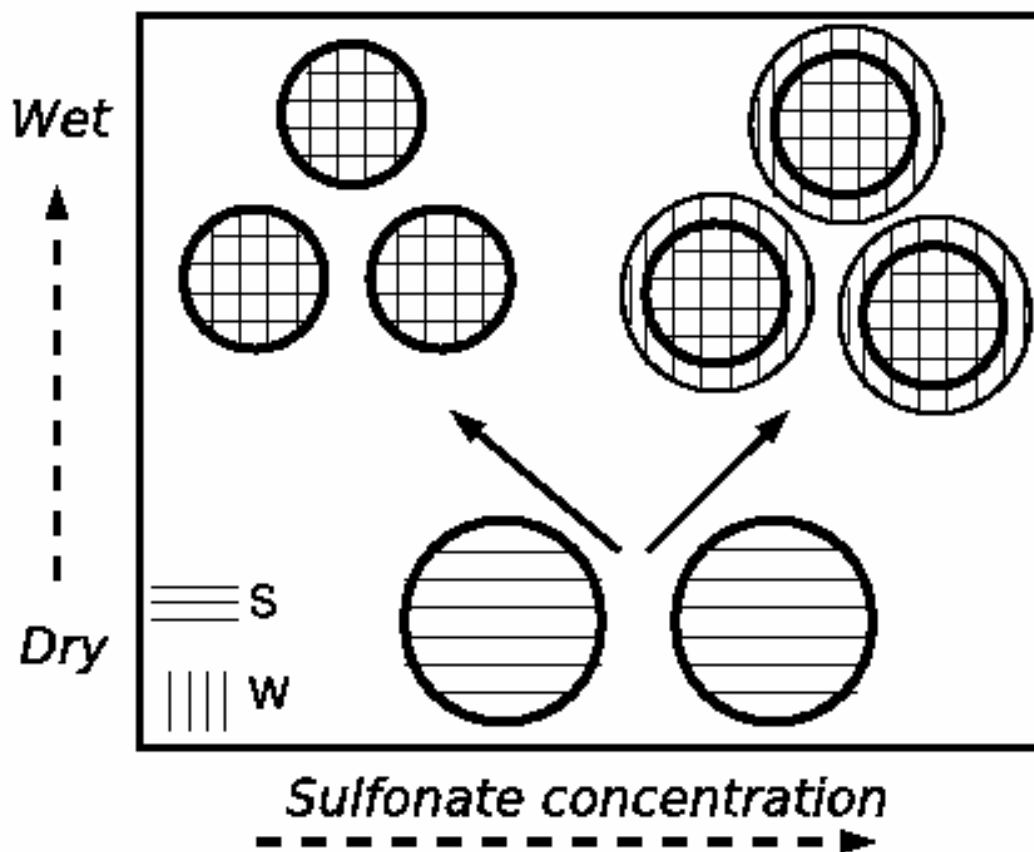Figure 14: (Color online) Mean squared displacement of protons as a function of time for Runs 2–4.

Figure 15: Schematic illustration of the multiplet hydration. At a low sulfonate concentration the hydrated multiplets consist of sulfonates and water molecules. At a higher sulfonate concentration each of the multiplets is surrounded by a water shell. The splitting of dry multiplets into smaller hydrated multiplets is also sketched. Vertical/horizontal hatching is used for the water (W) and the sulfonate (S) areas of the multiplet.